

Nanocomposites

ISSN: 2055-0324 (Print) 2055-0332 (Online) Journal homepage: www.tandfonline.com/journals/ynan20

3D reconstruction and correlative imaging of graphene nanocomposites: combining scanning electron and optical microscopies

Yuhan Li & Milo S. P. Shaffer

To cite this article: Yuhan Li & Milo S. P. Shaffer (2026) 3D reconstruction and correlative imaging of graphene nanocomposites: combining scanning electron and optical microscopies, Nanocomposites, 12:1, 24-41, DOI: 10.1080/20550324.2026.2655060

To link to this article: https://doi.org/10.1080/20550324.2026.2655060

© 2026 The Author(s). Published by Informa UK Limited, trading as Taylor & Francis Group.

View supplementary material

Published online: 17 Apr 2026.

Submit your article to this journal

Article views: 672

View related articles

View Crossmark data

Full Terms & Conditions of access and use can be found at
https://www.tandfonline.com/action/journalInformation?journalCode=ynan20

NANOCOMPOSITES
2026, VOL. 12, NO. 1, 24–41
https://doi.org/10.1080/20550324.2026.2655060

Taylor & Francis
by informa

RESEARCH ARTICLE

OPEN ACCESS Check for updates

3D reconstruction and correlative imaging of graphene nanocomposites: combining scanning electron and optical microscopies

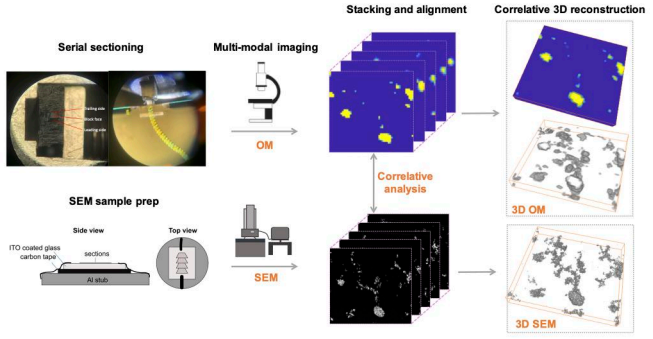
Yuhan Li[a,b] and Milo S. P. Shaffer[a,c]

[a]Department of Materials, Imperial College London, South Kensington Campus, London, SW7 2AZ, UK; [b]Institute for Composites Science Innovation (InCSI), School of Materials Science and Engineering, Zhejiang University, Hangzhou, 310058, China; [c]Department of Chemistry, Molecular Sciences Research Hub (MSRH), 82 Wood Lane, Imperial College London, London, W12 0BZ, UK

ABSTRACT

Microscopy is routinely applied to characterize nanomaterials and nanocomposites. Optical microscopy (OM) and scanning electron microscopy (SEM) are frequently adopted for their simple sample preparation and efficient image acquisition. The majority of literature analyses rely on 2D surface imaging or cross-sectional imaging, often at a single magnification, although they may not be representative, due to the multiscale nature of the structures, as well as preparation and projection artifacts. This paper presents a comprehensive 3D imaging workflow combining serial sectioning OM and SEM to obtain realistic volumetric nanocomposite structures. The relationship between SEM acceleration voltage, electron penetration depth, and image contrast is investigated to enhance sub-surface imaging. Correlative OM and SEM characterization is achieved through multimodal imaging and landmark-based registration. Multiscale reconstruction is demonstrated on three representative 'graphene' nanocomposite systems, providing rich datasets on dispersion, distribution, orientation, and morphology. The methodology presented is broadly applicable to other nanocomposites and hierarchical systems.

GRAPHICAL ABSTRACT



ARTICLE HISTORY
Received 15 July 2025
Accepted 30 March 2026

KEYWORDS
Nanocomposites; microscopy; serial sectioning; subsurface imaging; correlative characterization; 3D reconstruction; graphene; morphology

1. Introduction

In the ongoing development of carbon nanomaterials and their derivatives, nanocomposites have attracted particular attention, as a promising route to exploit exceptional intrinsic properties in a macroscopic form suitable for a broad range of applications [1,2]. The introduction of small loadings of carbon

CONTACT Milo S. P. Shaffer m.shaffer@imperial.ac.uk Department of Materials, Imperial College London, South Kensington Campus, London, SW7 2AZ, UK

Supplemental data for this article is available online at https://doi.org/10.1080/20550324.2026.2655060

© 2026 The Author(s). Published by Informa UK Limited, trading as Taylor & Francis Group.
This is an Open Access article distributed under the terms of the Creative Commons Attribution License (http://creativecommons.org/licenses/by/4.0/), which permits unrestricted use, distribution, and reproduction in any medium, provided the original work is properly cited. The terms on which this article has been published allow the posting of the Accepted Manuscript in a repository by the author(s) or with their consent.

nanofillers (such as carbon nanotubes or graphene-related materials) into polymer matrices offers significant improvements in both mechanical and functional properties [3,4]. However, the performance typically plateaus or reverses at increasing filler loading, a limitation often attributed broadly to 'poor dispersion' or 'agglomeration' effects. Further advances demand a more rigorous understanding of nanocomposite microstructure and the associated structure-property relations [5–7]. Characterization is typically challenging both due to the wide range of lengthscales involved and the relatively low contrast, in many cases, between carbon fillers and polymer matrices. The smallest intrinsic dimension of these high aspect ratio fillers is typically nanometers, the longest is typically microns, whilst agglomerates may be in the tens or hundreds of microns. The quality of nanofiller dispersion concerns the separation of individual particles; proper analysis requires resolution at the smallest particle dimensions and in three dimensions, since particle contacts in general may not lie in a given imaging plane. These contacts are critical for many properties, particularly percolation driven phenomena such as electrical conductivity, rheology, and load transfer pathways. Poor dispersion may be manifested by the presence of larger agglomerates at the scale of the longer dimensions of the particles, which may affect strength, reinforcement efficiency, toughness, and other defect based behavior. Finally, the distribution of the particles may vary at longer length scales, throughout the specimen, due to either inadvertent or intentional processing effects (including flows or applied fields), secondary/fractal agglomeration, or phase segregation (such as double percolation or Pickering emulsification) [8–10]. The multiscale nature of nanocomposite microstructure is difficult to study with a single technique, motivating the use of correlative analysis and other new methods [7]. Whilst dispersion issues arise in many, or arguably all, nanocomposites, they are particularly severe for high aspect ratio fillers, including carbon nanotubes (CNTs), graphene-related materials (GRMs), transition metal dichalcogenides (TMDs), and others. Network analysis of such nanocomposites [11] requires detailed knowledge of structural characteristics, such as dispersion, orientation, and local nanofiller morphology across multiple lengthscales and in three dimensions [7].

Conventional microscopies, such as optical microscopy (OM), scanning electron microscopy (SEM), and transmission electron microscopy (TEM), have been widely applied to carbon nanocomposites. Generally, samples are 2D, either viewed in projection (TEM, OM) or as a polished/fracture surface (OM, SEM), often with a limited range of magnifications and extent of statistical sampling. The microstructure is most often described qualitatively, though a variety of approaches to quantify dispersion have been developed [12–15]. Comparisons of different microscopies or magnifications support some commentary on the multiscale nanocomposite structure, but capturing the real volumetric structure experimentally has been challenging. As an alternative, multiscale modeling and simulation methods have been adopted to build 3D models and predict the behavior of nanocomposites [16–18]. In recent years, a variety of techniques have been explored as means to probe the 3D internal structure of carbon nanocomposites.

Confocal laser scanning microscopy (CLSM) enables nondestructive 3D imaging of materials or biological tissues through optical sectioning, with higher resolution than conventional OM [19]. 3D reconstructions of CNT nanocomposites, over the length scale of tens to hundreds of micrometers, have been achieved using both reflection-mode and fluorescence-mode imaging [12,20]. However, 3D CLSM imaging requires optical transparency, limiting the application to nanocarbon nanocomposites with relatively small filler loadings ($\leq\sim$0.5 wt% for CNT nanocomposites) and shallow depths. At a similar length scale, X-ray computed tomography (X-ray CT) has been applied to reconstruct the 3D microstructure of graphite (lateral size: 5–25 μm) nanocomposites [21]. Graphite platelets were segmented and classified based on their orientation and morphology inside the epoxy matrix [22,23]. However, the broader application of X-ray CT has been limited, especially in carbon nanocomposites, due to the limited contrast between carbon nanoparticles and polymer matrices, often requiring intense image processing in the reconstruction stage [24].

At higher (nanoscale) resolution, scanning transmission electron microscopy (STEM) tomography provides detailed analysis of particle packing and connectivity (i.e. of carbon nanotubes in epoxy [25]); however, the imaged volume is restricted to the scale of hundreds of nanometers, which may not even capture whole single particles. SEM-based 3D techniques cover a wide magnification range and are, in principle, especially suitable for multiscale characterization of nanocomposites. Although serial array tomography is relatively widely applied in 3D imaging and correlative characterization of biological

systems, it is only rarely applied in the context of nanocomposites [26–28]. Previously, serial block face SEM imaging has been used by our group to trace the trajectories of carbon nanotubes in nanocomposites, bridging the resolution gap between OM and (S)TEM [29,30]. More generally, by combining a variety of techniques, it is possible to access complementary information on nanocomposite architectures both at high resolution and across wide fields of view [31]; however, truly correlated multiscale characterization of carbon nanocomposites is rare.

This study develops multiscale serial sectioning-based 3D characterization methods on archetypal graphene nanocomposite systems, with different characteristic flake sizes. This technique involves the cutting and preservation of serial nanocomposite sections using a laboratory ultramicrotome, followed by imaging using OM and SEM under carefully optimized conditions. Correlative imaging and registration techniques are explored to obtain full multiscale 3D nanocomposite morphologies. This study aims to demonstrate the importance of 3D correlative characterization for understanding the microstructure of nanocomposites, establish suitable protocols for such systems, and provide useful multiscale datasets for representative systems.

2. Materials and methods

2.1. Preparation of graphene nanocomposites

Three types of starting graphene materials with different lateral sizes were selected as representative nanofillers (see SEM images in Figure S1). Graphene nanoplatelets (GNP, lateral size∼500 nm) were obtained from Cambridge Nanosystems UK (G3 Grade Graphene Powder). Exfoliated graphite platelets (EG, lateral size: 1–5 μm) were provided by Thomas Swan (Elicarb Materials Grade Graphene Powder SP8082). The literature is inconsistent on the definition of terms for graphene-related materials (see the *Carbon* editorial on nomenclature) [32]; here, we use the term GNP to describe thin particles (thickness: 0.02 μm) with sub-micron lateral dimensions (∼500 nm) grown directly by CVD, and the term EG to describe larger platelets (lateral size: 1–5 μm, thickness: 0.5 μm) generated by high shear exfoliation of graphite. GNP/epoxy nanocomposites and EG/epoxy nanocomposites were prepared from graphene powders and Embed 812 epoxy resin (TAAB Laboratories), hardener dodecenylsuccinic anhydride (DDSA), methyl nadic anhydride (MNA), and accelerator benzyldimethylamine (BDMA) using a solution mixing method [33]. The Embed 812 formulation used a mass ratio (TAAB 812:DDSA:MNA:BDMA) of 46.1:11.5:48.5:3.8. This resin was selected as a representative epoxy, particularly suited to microtome sectioning. The graphene materials and the epoxy resin were first dispersed separately in ethanol, then mixed and sonicated before solvent evaporation. Hardeners and accelerators were added, and the mixture was transferred to a flat silicone rubber embedding mold, degassed, and cured at 60 °C for 24 h. Graphite/epoxy nanocomposites were supplied by Fraunhofer ICT (Karlsruhe, Germany), contain graphite flakes (GF, 40 μm in lateral size) produced by Avanzare Innovación Tecnológica in an epoxy (resin RIMR 426, hardener RIMR 433, EPIKOTE) matrix. This matrix represents a conventional structural epoxy system. The three types of graphene-related nanocomposites were labeled as GNP/epoxy, EG/epoxy, and GF/epoxy, respectively.

2.2. Serial sectioning and preparation of SEM samples

Serial sectioning of graphene nanocomposites was performed on a laboratory ultramicrotome (PowerTome XL, RMC™). The block face of a specimen was first trimmed into a trapezoid pyramid shape (base width, height $<$ 1 mm), with the side faces painted with Scotch-Weld™ contact adhesive (3M™)/xylene solution (1:2). Serial sections of graphene-related nanocomposites (hundreds of nm) were cut sequentially using a diamond knife (ultra 45°DiATOME), collected and preserved on ITO-coated glass slides (Sigma-Aldrich), allowing subsequent repetitive/multi-modal imaging. The effect of mechanical sectioning on morphology observation is discussed in the ESI (Section S2). Under the primary conditions used in this work (1 wt% loading; section thickness of a few hundred nanometers), the observed effects are limited to typical faint mechanical knife marks. No evidence of graphene platelet fragmentation or systematic distortion attributed to sectioning was observed (supported by SEM). No obvious systematic

section compression was apparent at the length scales analyzed. For OM imaging, the ITO-coated glass slide was placed directly on the OM sample stage. For SEM imaging, the ITO-coated slide was fixed onto an aluminum stub using carbon tape and imaged without any conductive coating. The serial stacks used for correlative analysis comprised 23 (GNP/epoxy), 23 (EG/epoxy), and 20 (GF/epoxy) consecutive sections; sections were excluded only if mechanically damaged or if the region of interest (ROI) could not be reliably tracked. Section-thickness profiles and variability are provided in the ESI (Figure S2). *Z*-scaling was based on the mean section thickness of each serial stack.

2.3. Characterization

A Leica DM2700 Polarizing microscope (Leica, Germany) was used to image the nanocomposite serial sections in transmission mode using a 50× objective (500× total magnification). The light intensity, quantified as the average grayscale value, was calibrated for each measurement using a calibration slide with 0.1 and 1.0 neutral density filters. The illumination level was carefully monitored, consistently maintained throughout the measurements. Live image stitching was performed with dedicated scanning software (Microvisioneer, Germany) which allowed stitched optical images of a whole series of sections to be obtained by manually moving the sample stage. The thicknesses of serial sections were measured from depth profiles in atomic force microscopy (AFM) images obtained using a hpAFM (NanoMagnetics Instruments). For each specimen, the average thickness was measured from 8 to 10 randomly selected sections. A Zeiss LSM 800 confocal laser scanning microscopy was used to assess the surface morphology of serial sections (reflection mode). A Zeiss Leo Gemini 1525 field emission gun SEM (In-lens imaging mode, accelerating voltage 1 kV) was used to characterize the morphology of graphene particles and graphene nanocomposites (fracture surface). A Zeiss Auriga field emission SEM was utilized for imaging the serial sections of graphene nanocomposites. SEM images were acquired at 3–6 kV using an InLens detector (WD: 5–6 mm), with frame averaging enabled to reduce noise. Brightness/contrast were adjusted linearly for visualization.

2.4. Software

Fiji was used for pre-processing of optical microscopy and SEM images (Section S1, ESI) [34,35]. Multimodal OM and SEM registration was achieved using the BigWarp plugin [36]. Custom MATLAB (Mathworks) scripts were used for concentration mapping of OM images. Avizo (Thermo Fisher Scientific) was used for 3D volume rendering/visualization. Monte-Carlo simulations of electron trajectories under different SEM beam acceleration voltage were performed using the CASINO v2.5.1 software [37].

3. Results and discussion

Three starting materials were selected as typical examples of commercial 'graphene'-based materials, more properly considered as graphene nanoplatelets (GNPs) or few layer graphenes (FLGs) [32], with characteristically different flake sizes (∼0.5, 5, and 40 microns). Graphene-related fillers of different characteristic flake sizes present potentially different dispersion/distribution behavior and different imaging challenges. The powders were dispersed into epoxy resin (detailed in Section 2.1), one of the most common classes of nanocomposite matrices.

3.1. Limitations of conventional SEM surface imaging

Typically, nanocomposite morphology is assessed by SEM surface imaging of bulk samples performed in secondary electron (SE) mode under low beam acceleration voltages [38]. Conductive coatings (sputtered metals) are usually applied to eliminate charging artifacts, providing pure topographic contrast, but reduce resolution and can obscure the nanostructures of interest, particularly on cut or polished specimens. As a result, many studies examine fracture surfaces, where topological features are retained; however, this approach adds further bias to the analysis, since not all particles necessarily sit proud of the surface, whilst the fracture process itself is likely to selectively locate to agglomerates or other defect

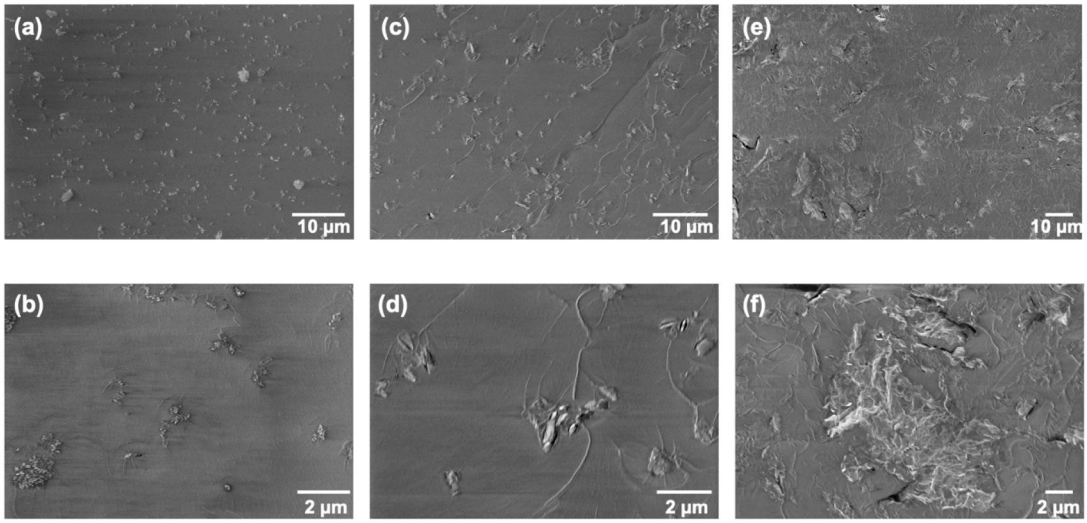


Figure 1. SEM images of uncoated fracture surface of the three types of graphene-related nanocomposites, captured at an electron beam acceleration voltage of 1 kV. (a,b) 1 wt% GNP/epoxy nanocomposites. (c,d) 1 wt% EG/epoxy nanocomposites. (e,f) 1 wt% GF/epoxy nanocomposites.

features. A less common alternative avoids coatings, instead using voltage contrast between the conductive nanofillers and polymer matrices to reveal additional detail [39,40]. To contextualize the challenges of characterizing carbon nanocomposites, the fracture surfaces of the three 'graphene'-based systems were examined, uncoated, using an In-lens SE detector with an acceleration voltage of 1 kV. The general distribution of the various graphene nanofillers was observed (Figure 1). However, the image contrast between graphene and epoxy is relatively low, making it difficult to resolve the morphologies of individual graphene nanoplatelets or inter-particle contacts. The 2D images provide information of a limited surface area and do not necessarily represent the volumetric structure. In addition, the imaging depth is voltage-dependent, although this sensitivity is frequently ignored in the field. Increasing accelerating voltage can enhance subsurface sensitivity and reveal near-surface embedded conductive networks or inter-particle connectivity that are not evident in conventional surface SEM images. However, the practical imaging depth in polymer nanocomposites remains limited to the sub-micrometer range and is strongly constrained by charging in the insulating matrix (Figure S3), which can bias contrast and degrade image quality [40,41]. As shown below, this limitation can be addressed by microtoming thin nanocomposite slices, which brings deeper regions within the SEM information depth when supported on a conductive substrate. Consecutive nanocomposite slices can be collected using the serial sectioning technique, allowing for investigation of the microstructure at different sample depths.

3.2. SEM imaging of serial sections

Thin (hundreds of nanometers) serial sections of graphene-related nanocomposites were obtained by ultramicrotomy and preserved on ITO-coated glass for imaging and 3D construction. SEM-based surface and subsurface imaging, while widely used for studying the morphology of bulk or powder carbon nanocomposites, is known to be influenced by various factors, including beam energy, filler dispersion, and sample thickness [38,41]. Initially, systematic investigations were performed to understand the interplay between acceleration voltages (3–6 kV), slice thicknesses (cutting thickness, 100–300 nm), and image quality (contrast and resolution).

In this study, the serial sections were left uncoated to avoid coating-related artifacts and to image the particles within the slices. In contrast to the surface images of bulk samples (Figure 1), the SEM images of 200 nm thin slices exhibited significantly enhanced contrast under all investigated acceleration voltages (3–6 kV, Figure 2); different regions were imaged for this comparison to avoid any effect of charging history. Beam-induced charging artifacts (square patches in Figure 2(b)) were occasionally observed during imaging, particularly upon repeated scanning or at higher magnification. These artifacts

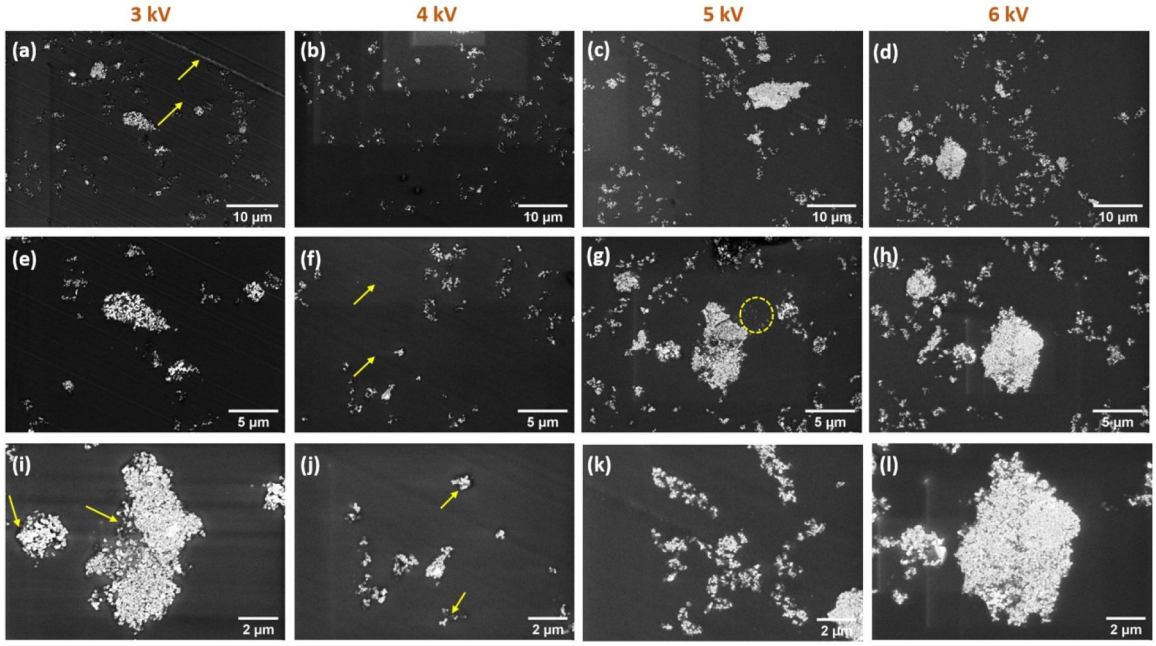


Figure 2. SEM images of uncoated 1 wt% GNP/epoxy nanocomposite sections (200 nm thick) captured at different electron beam acceleration voltages. (a,e,i) 3 kV. (b,f,j) 4 kV. (c,g,k) 5 kV. (d,h,l) 6 kV. Regions of knife marks and local charging are indicated by yellow arrows, and small particle features are highlighted by the yellow circle.

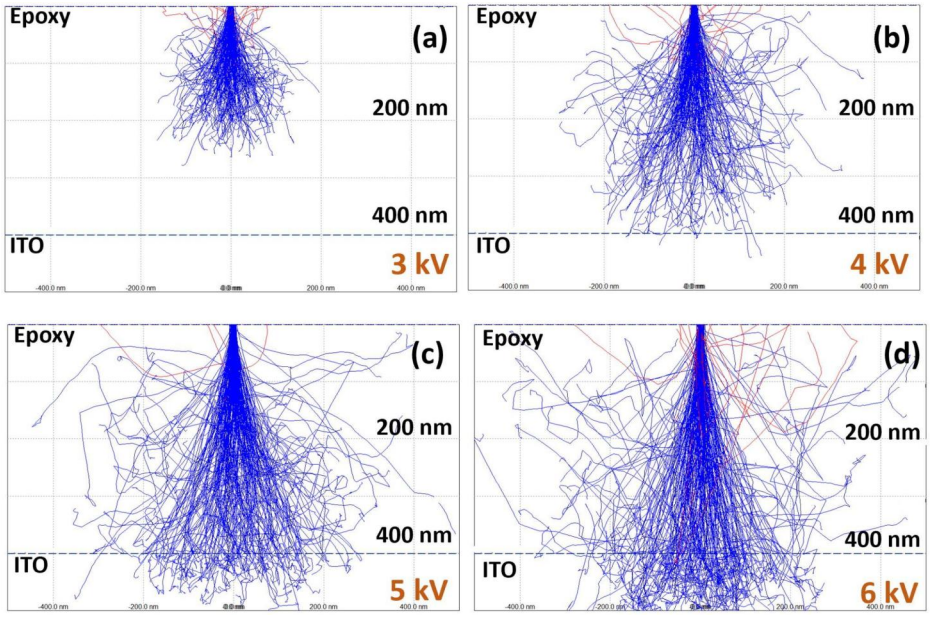


Figure 3. Monte Carlo simulations of electron trajectories in epoxy (a–d) using different beam acceleration voltages. Top layer: epoxy or graphene sample with a thickness of 400 nm, bottom layer: ITO substrate. Primary electrons entering the samples are labeled in blue; backscattered electrons are labeled in red.

were minimized by reducing dwell time and avoiding repeated scans of the same area during acquisition. At the lower voltages (3–4 kV), local charging and defects caused by cutting (arrowed regions in Figures 2(a–j)), such as knife marks, were observed. The best image quality (sufficient contrast, absence of surface artifacts) was achieved above 5 kV, where even small graphene particles were clearly resolved (Figure 2(g)). Having selected an accelerating voltage of 5 kV for further studies, the effect of slice thickness was examined (Figure S6); while both 100 nm and 200 nm sections showed good contrast, increasing the slice thickness to 300 nm introduced local charging around graphene particles (Figure S6(f)).

The penetration depths of incident electrons during SEM were visualized by Monte Carlo simulations of electron trajectories in both epoxy (Figure 3) and graphene (Figure S7) [37]. These simulations describe the electron-sample interaction volume; practical SEM resolution additionally depends on probe size and focusing/stigmation conditions, which also vary with landing energy. Although the penetration depth is shorter in graphene, the low loading (1 wt%) means that the epoxy results are more representative. The electron penetration depth and interaction volume increase with beam acceleration energy in both epoxy and graphene. At low acceleration voltage (3–4 kV), local charging can occur due to the restricted penetration depth of electrons relative to the sample thickness. Above 5 kV, the electron penetration depth exceeds the 300 nm slice thickness; as a result, the incident electrons begin to be transferred to the conductive substrate reducing sample charging, as observed in the imaging experiments. While higher beam energies are feasible, an intermediate acceleration voltage range (5–6 kV) was chosen in this study for slice thicknesses of 100–300 nm to avoid matrix damage at higher beam energy [29].

3.3. 3D serial sectioning SEM workflow

Building on established array-tomography workflows [27,30,42,43], a comprehensive workflow was adapted and integrated for graphene nanocomposites and is summarized in Figure 4. The successful volume reconstruction relies on two key steps: the acquisition of parallel sections by ultramicrotomy and the imaging of targeted regions in consecutive sample slices (Figures 4(b–d)). In some cases, pre-processing of images (S3, ESI) may be necessary for improving image quality (Figure 4(d)). Following image alignment and resampling, an image series with continuous structural features is generated, as shown in the image montage (Figure 4(e)). Finally, 3D visualization of the structure is achieved (Figures 4(f,g)). Additional segmentation, quantitative or correlative analysis can be performed to provide detailed structural information. Beyond microscopy-based morphological contrast, spectroscopic imaging (e.g. Raman mapping and electron-energy/elemental spectroscopy) can add chemically specific information for carbon nanomaterials embedded in polymers and has been combined with serial-section imaging in recent studies [44–47]. Such approaches provide a complementary direction for extending the present workflow where phase-specific identification is required.

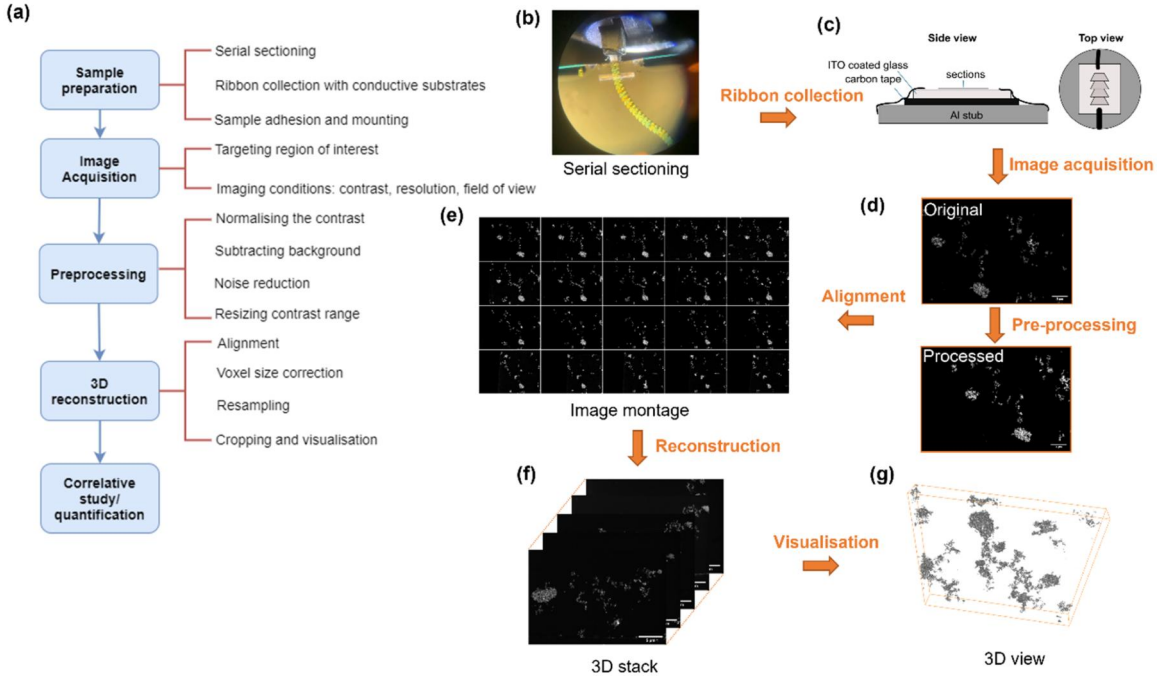


Figure 4. Framework for 3D reconstruction of nanocomposites by serial sectioning SEM. (a) Workflow showing the main steps. (b) Sample preparation by the serial sectioning process. (c) Sample adhesion and mounting. (d) Image acquisition and pre-processing. (e) Image series alignment. (f) 3D stacking. (g) 3D visualization.

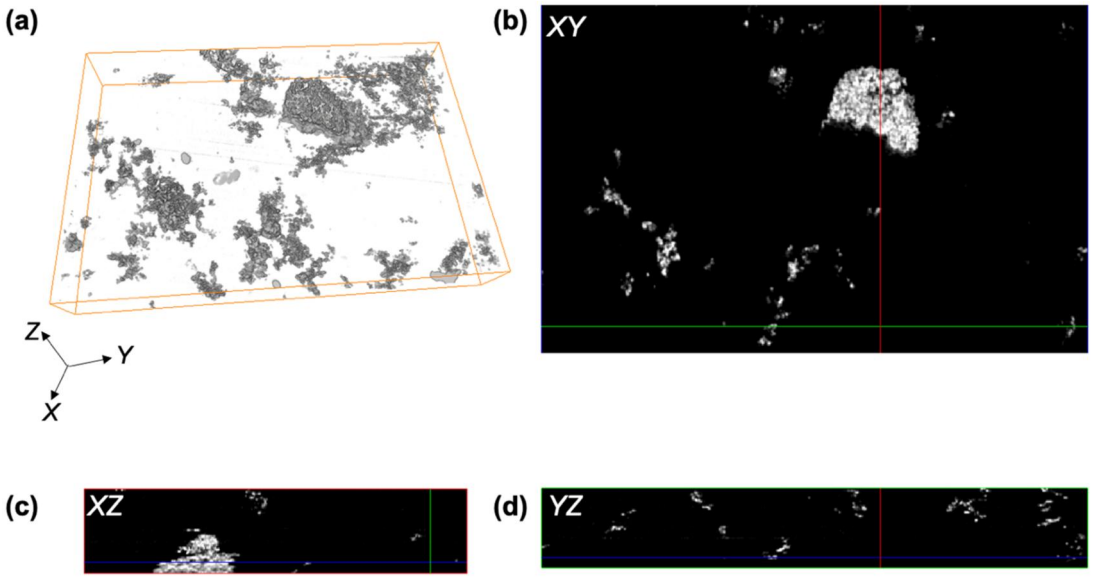


Figure 5. 3D reconstruction of 1 wt% GNP nanocomposites using SEM images captured at 5 kX magnification. (a) 3D view. Orthogonal view: (b) XY view. (c) XZ view. (d) YZ view. SEM images of serial slices were aligned and registered into a stack for 3D reconstruction. 3D visualization rendered in Avizo.

3.4. Example of image processing and reconstruction

The successful application of this workflow is illustrated with the 1 wt% GNP epoxy nanocomposites. Section-to-section alignment was performed using SIFT feature matching with a least-squares fit to a global rigid/affine transform (translation/rotation and, where required, scale/shear); no non-rigid morphing was applied to avoid distorting filler features. By comparing overlapping regions of neighboring sections before and after image alignment, the registration quality can be verified (Figure S9). The resulting transforms were applied across the full image stack to generate an aligned 3D dataset with continuous depth features (Figure 5). The voxel size in the reconstructed volume was defined by the in-plane resolution (55 nm/pixel) of SEM images and the average thickness of sections (108 ± 18 nm, measured by AFM). After resampling, with *Z*-axis interpolation using the Lanczos kernel method [48], the voxel resolution was $55 \times 55 \times 54$ nm. The images were reconstructed into a total volume of $32.3 \times 21.6 \times 4.7$ µm. The resulting 3D dataset ($593 \times 396 \times 88$ voxels) provides a high-resolution reconstruction of particle arrangement, as illustrated in both 3D and orthogonal views (Figure 5).

It is possible to visualize the local organization of nanoparticles at higher magnification to provide fine structural details (Figure 6). The acquisition of images from low to high magnifications enables the generation of a series of 3D images with varying sizes and resolutions. This imaging process is particularly useful for correlative characterization, as it enables tracked analysis across different length scales (see Section 3.5).

3.5. Correlative methodology for multiscale study of graphene-related nanocomposites

The serial sectioning technique preserves sample slices for repetitive imaging by both light microscopy and electron microscopy; depositing sections on an ITO-coated glass substrate maintains transparency for transmission OM, and electrically conductivity to minimize charging in SEM. We previously developed a calibrated OM method to determine real nanoparticle concentrations in nanocomposite slices, which we combine here with correlated SEM data, in both 2D and 3D, at multiple scales [29,49]. The optical concentration mapping method generates the absolute filler concentration of each pixel by analyzing the absorbance of OM images and applying the Beer-Lambert law (Figure S10). This method is particularly useful for investigation of macro-scale distributions of graphene in nanocomposites, since the OM images are rapidly stitched over large areas (Figure S11). The serial sectioning SEM technique, on the other hand, provides high-resolution information, including on dispersion, individual particle structure,

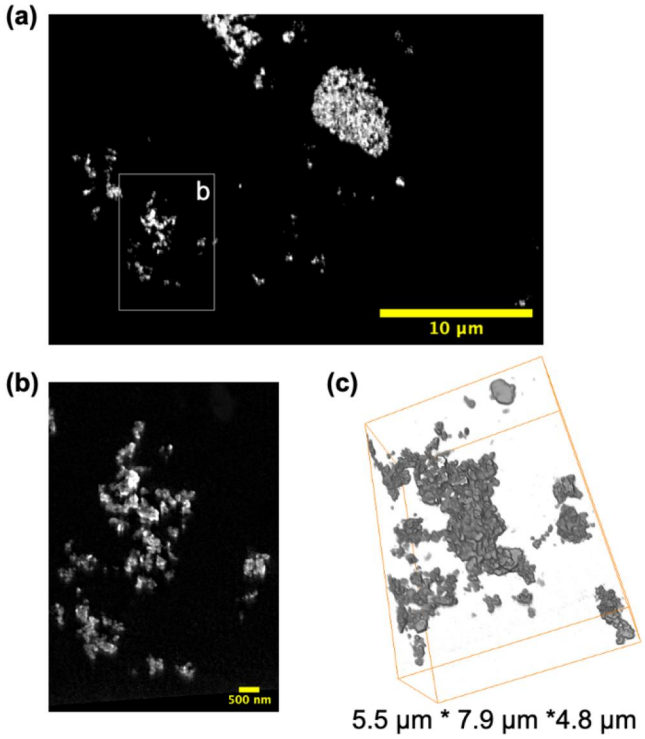


Figure 6. High magnification (20 kX) 3D reconstruction of particle organization (1 wt% GNP nanocomposites). (a) The top slice of the stack in Figure 5. (b) A sub-region selected from (a) and imaged at 20 kX magnification. (c) 3D reconstruction of the sub-region. 3D visualization rendered in Avizo.

and inter-particle contacts. The correlative use of optical concentration mapping and serial sectioning SEM is, therefore, promising for achieving multiscale structural reconstruction of graphene-related nanocomposites. Here, correlative OM-SEM refers to registered imaging of the same serial sections, where OM provides rapid large-area screening (and concentration mapping) to target ROIs and SEM provides high-resolution morphology/connectivity of the same regions.

3.5.1. Targeting ROIs

In order to correlate the OM & SEM data, target ROIs have to be identified efficiently under different imaging modes. The process is illustrated first for 1 wt% GNP/epoxy nanocomposites (Figure 7). Initially, a stitched optical scan of serial sections provides an overview of the sample at a relatively low magnification (Figure 7(a)). Once the ROIs are identified, the corresponding regions can be located and imaged under SEM at equivalent magnification (Figures 7(b,e)) or then studied at higher magnification, as needed. Local features identified at relatively high SEM magnifications can be traced back to the original optical scan conveniently (Figures 7(a,e–g)). The entire set of 3D slices is preserved throughout the process, allowing any ROIs to be re-imaged or new ROIs to be selected, guided by the stitched optical scan.

3.5.2. Correlative analysis

Once the targeted ROIs have been imaged, the correlation between SEM images and corresponding optical concentration maps can be analyzed through a supervised multi-modal registration method. Landmark-based registration was performed using the BigWarp plugin in Fiji (S4, ESI). OM-SEM registration was performed on the same physical sections using landmark/feature matching, and verified by overlaying corresponding structural features in both modalities. OM and SEM images were registered to the same physical sections and compared within the same ROI. The presence of well-aligned agglomeration features in the yellow channel showed the successful correlation between the two imaging modes (shown separately as red & green channels) in a single 2D slice (Figure S13). For 3D correlative analysis,

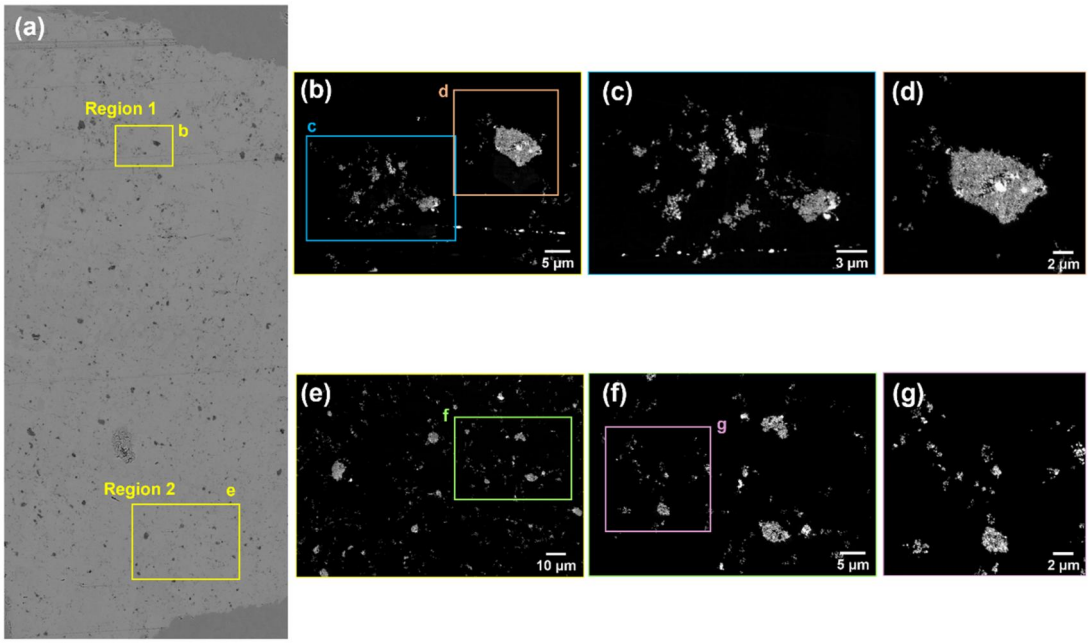


Figure 7. Correlative SEM and OM imaging targeting ROIs and multiscale imaging (1 wt% GNP/epoxy nanocomposites, 100 nm sections). (a) Stitched optical scan of an individual sample slice. (b–d) SEM images of local structures captured from region 1 at different magnifications. (e–g) SEM images of region 2 captured at different magnifications. Color boxes in (a,b,e,f) depict regions selected for imaging at increasing magnifications.

a slice-by-slice registration method was employed, as both optical and SEM images were already acquired for each nanocomposite slice.

3.6. 2D and 3D correlative analysis of representative graphene-related nanocomposites

To demonstrate its versatility and capability, the correlative serial sectioning-based 3D reconstruction technique was applied to the three complementary examples: GNP/epoxy, EG/epoxy, and GF/epoxy nanocomposites. Here, the motivation is to resolve the real filler architecture (distribution, agglomeration, and inter-particle connectivity) over representative volumes, since these features dominate processing heterogeneity and percolation/defect driven behavior in graphene nanocomposites.

3.6.1. Graphene nanoplatelet/epoxy nanocomposites

Starting with small lateral size (0.5 µm, 1 wt% GNP/epoxy), 2D correlation was successfully applied between the optical concentration mapping and SEM images of thin serial sections (108 ± 18 nm) at different SEM magnifications (Figure 8). At 2 kX magnification, the GNP distribution was observed in the correlated field of view (FoV), using both OM and SEM (Figures 8(a–c)). The larger features, which are attributed to agglomerates of graphene nanofillers, were all well correlated. As the magnification is increased to 10 kX (Figures 8(d–f)) and then 50 kX (Figures 8(g–i)), the resolution limit of OM becomes increasingly obvious, with numerous new features appearing in the green (SEM) channel, not visible in the OM (red) channel. While the general shape of an agglomerate can be seen from the optical micrograph, the organization of graphene nanoplatelets inside the agglomerate is only resolved by SEM, providing additional detail on the local structure at 70 and 100 kX (Figures 8(j,k), respectively).

By applying the 2D correlation to the full series of images captured at 10 kX (example slice shown in Figures 9(a–c)), a correlated 3D volume of the selected ROI (21.9 × 19.6 × 2.5 µm, 804 × 718 × 80 voxels), was visualized using both OM and SEM (Figures 9(d,e)). The overlapped region in the 2D 'composite' image of the first slice from the stack again showed both large correlated features and small particles resolved only by SEM (Figure 9(b)). Notably, the features absent in the 2D optical images, once reconstructed into a 3D volume, contributed to a locally connected structure (Figure 9(d), highlighted by a pink arrow). An animated rotation of the 3D structure is provided to highlight the local structure in

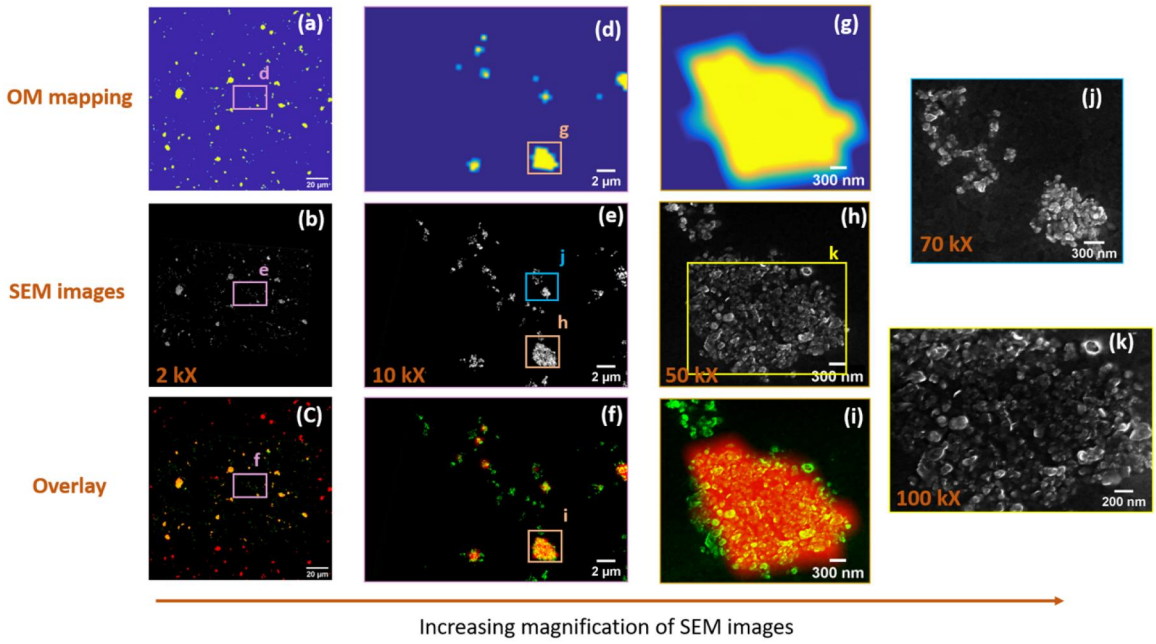


Figure 8. 2D correlative analysis of optical maps and SEM images in 1 wt% GNP/epoxy nanocomposites, combined with examples of higher local SEM magnification. (a,d,g) Corresponding optical maps of the correlated regions. (b,e,h,j,k) SEM images of the targeted regions. (c,f,i) Correlated 'composite' images illustrating the overlay between OM maps and SEM images (red channel: OM map, green channel: SEM images). Color boxes in (a–f,h) depict regions selected for imaging at increasing magnifications.

more detail (Video S1). The 3D correlative characterization enables the precise reconstruction of the internal structure, combining both overall concentrations and revealing the details of the local graphene network essential for understanding the properties of nanocomposites [25,50].

3.6.2. Exfoliated graphite/epoxy nanocomposites

The same correlative approach was then applied to EG nanocomposites with an intermediate flake size (5 μm). However, the ultramicrotomy became more challenging; consequently, serial sections with a thickness of 322 ± 32 nm were used for 3D analysis. A strong correlation between the two imaging methods were observed for almost all particles at various SEM magnifications, as might be expected given that the lateral size of graphene nanoplatelets falls within the resolution range of both techniques (Figure 10). However, at relatively high magnifications, SEM images revealed the orientation of the graphene nanoplatelets, whereas no such information can be seen in the corresponding optical map (Figures 10(g,h)). In comparison, the platelet features appear to be larger in the optical image (Figure 10(i)), due both to the resolution limit and the projected width of the platelet through the thickness of the slice. The layer morphology of individual nanoplatelets can be resolved in SEM at 50 kX and 100 kX (Figures 10(j,k)). The implication of the correlative analysis, here, is thus different to that of GNP/epoxy nanocomposites. The optical method depicts the general distribution of graphene, but high-resolution SEM imaging provides the morphological information (e.g. flake structure, orientation) of the individual nanoparticles.

3D correlative analysis was again successfully performed by combining OM and SEM datasets (18.5 × 16.1 × 7.4 μm, 679 × 591 × 230 voxels); for this intermediate flake size sample (5 μm, EG/epoxy) (Figure 11), animated slice-by-slice comparisons of the two imaging modes are available (Video S2). The 3D SEM dataset provides high-contrast details about the spatial arrangement and orientation of the platelets (Figure 11(d)). The corresponding 3D OM volume provides the spatial distribution of the particles, although at reduced resolution due to thickness averaging and obvious artifacts caused by knife marks (Figure 11(e)).

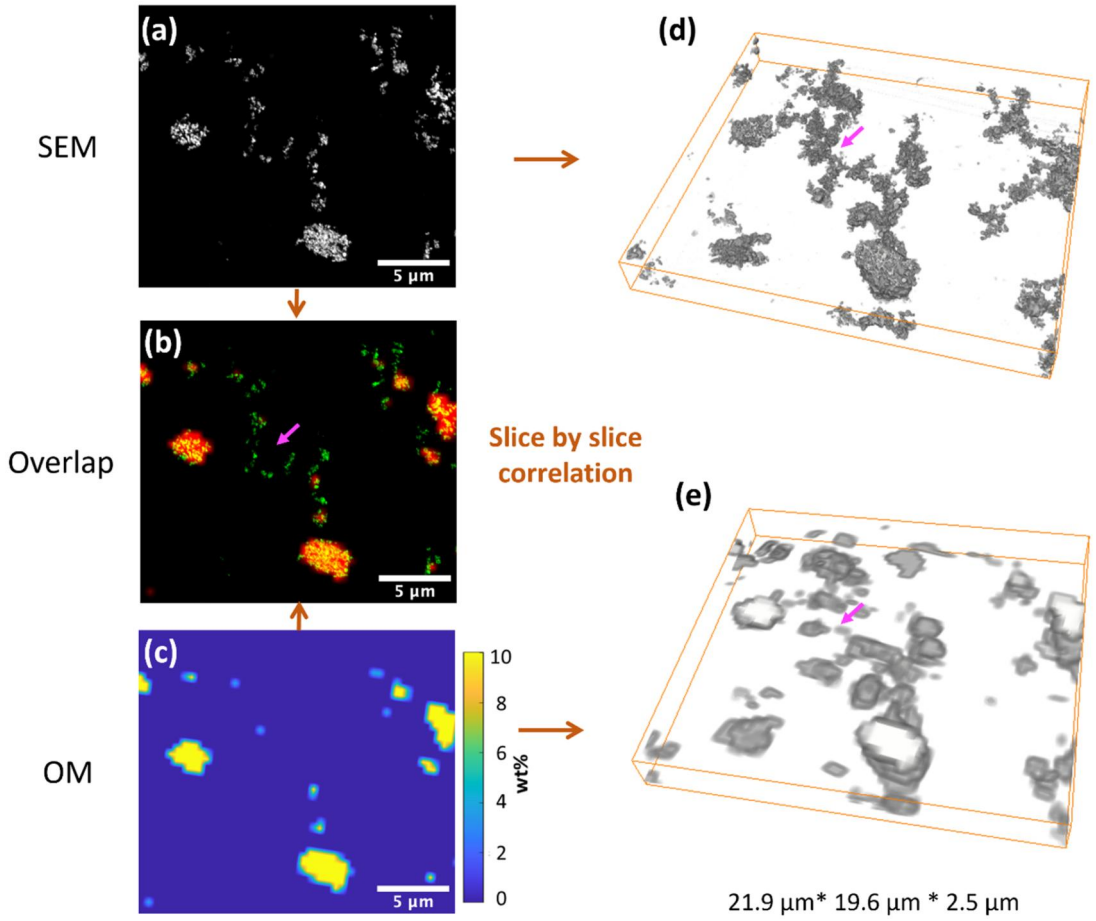


Figure 9. 3D correlative analysis of OM maps and SEM images for 1 wt% GNP/epoxy nanocomposites. (a) SEM image of the top slice from the stack. (b) Overlay of 2D SEM image and OM map. (c) OM map of the correlated region. (d) 3D reconstruction of the selected region from SEM images. (e) 3D reconstruction from OM images. The pink arrows indicate the local structures resolved exclusively by SEM. 3D visualization of datasets was achieved using the volume rendering function in Avizo. A 'volrenWhite' colormap was used for both OM and SEM datasets. To remove the background and improve 3D visualization, thresholding was applied to OM (threshold: 5) and SEM (threshold: 20) 3D datasets.

3.6.3. Graphite/epoxy nanocomposites

Graphite flakes are often used for mechanical reinforcements of polymer-based nanocomposites [3,23]. Correlative analysis was applied on serial sections obtained from graphite nanocomposites with a large flake size (40 µm, GF/epoxy). Again, a relatively large slice thickness (average thickness: 282 ± 27 nm) was used, due to the challenges in sectioning thin slices of graphite nanocomposites. The 2D optical maps of serial sections revealed a diverse morphology (Figure 12(a)), displaying different degrees of flake stacking, curvature, and size. The internal layered flake morphology was clearly resolved in the SEM images (Figures 12(b,e)), even at low magnifications. Whilst the two imaging techniques were broadly well correlated and consistent, in the optical channel, the internal flake morphology was completely missing; the multilayer structures appear as large agglomerates (Figures 12(a,d)), and some thinner-layer graphite flakes were not resolved. At higher magnifications, SEM clearly revealed the wavy, curved multilayers that were not visible in OM (Figures 12(g–l)).

The difference between the two imaging modes was further investigated by comparing the reconstructed 3D structures (Figure 13). A good correlation was observed between OM and SEM reconstructions, as evidenced by the agreement of large flakes in the overlapping regions. The 3D SEM reconstruction ($39.4 \times 36.0 \times 5.6$ µm, $723 \times 660 \times 100$ voxels) again shows the variety of graphite flake morphologies, including high-resolution structural details such as smaller flakes and curved multilayers (Figure 13(d)). As a demonstration of quantitative analysis enabled by the reconstruction, an apparent

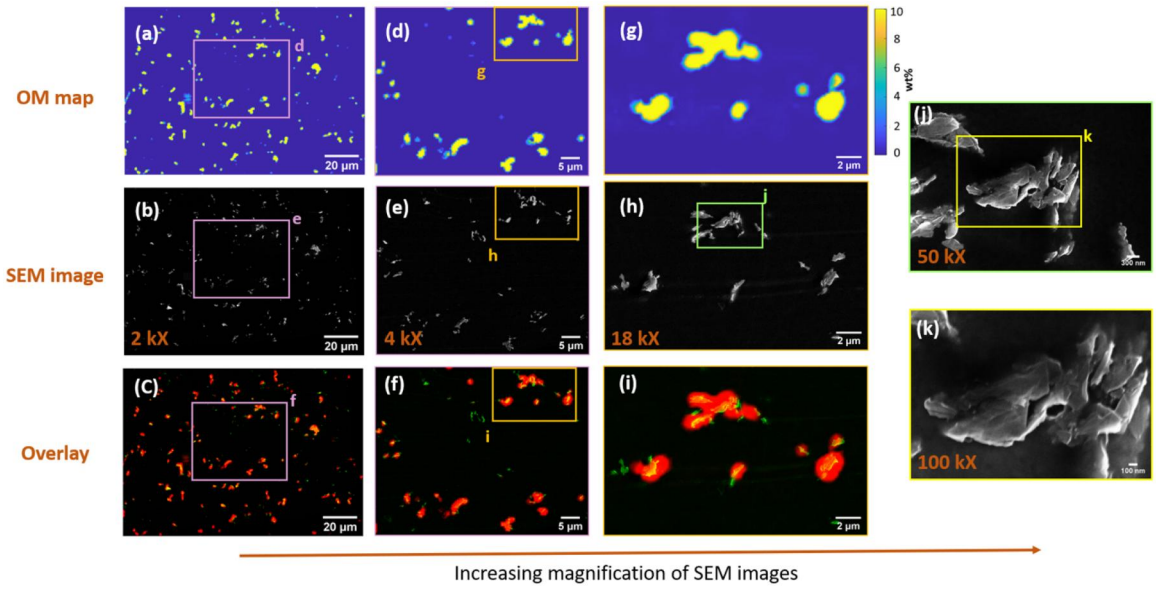


Figure 10. 2D correlative analysis of OM maps and SEM images in 1 wt% EG/epoxy nanocomposites , combined with examples of higher local SEM magnification. (a,d,g) Corresponding OM maps of the correlated regions. (b,e,h,j,k) SEM images of the targeted regions. (c,f,i) Correlated images illustrating the overlay of OM maps and SEM images. (red channel: OM maps, green channel: SEM images). Color boxes in (a–f,j) depict regions selected for imaging under increasing magnifications.

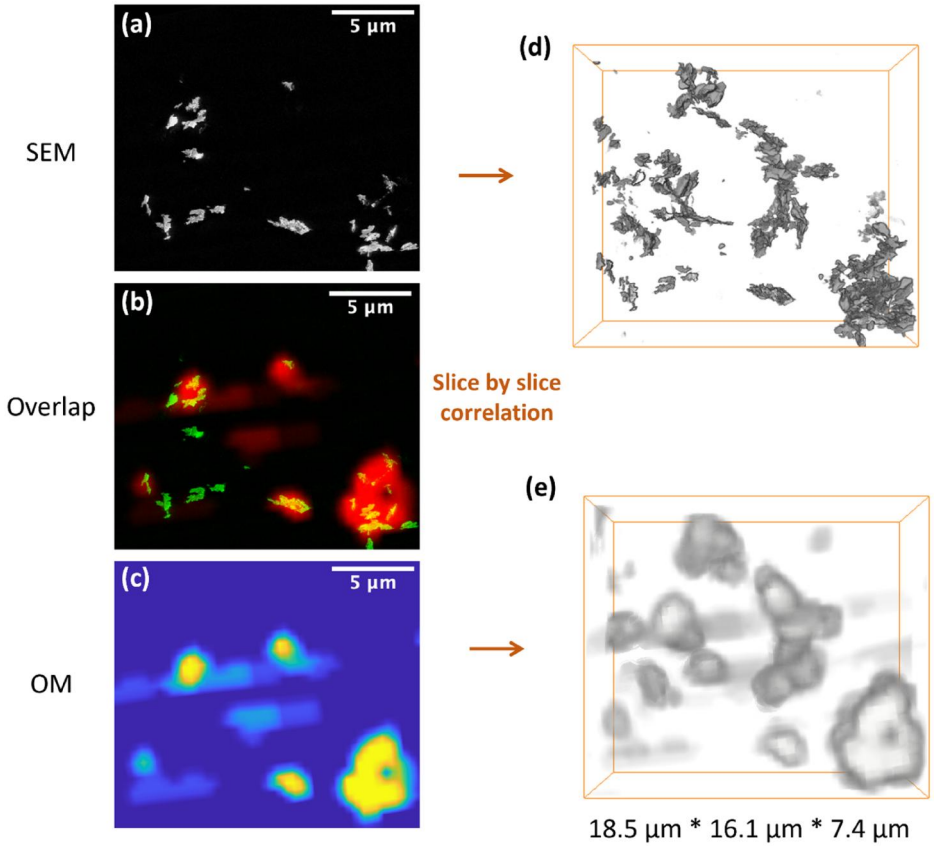


Figure 11. 3D correlative analysis of OM maps and SEM images in 1 wt% EG/epoxy nanocomposites. (a) SEM image of the top slice from the stack. (b) Overlay of SEM (green channel) and OM (red channel) images. (c) OM map of the top slice. (d) 3D reconstruction of the selected region from SEM images. (e) 3D reconstruction from OM maps (rendered in grayscale).

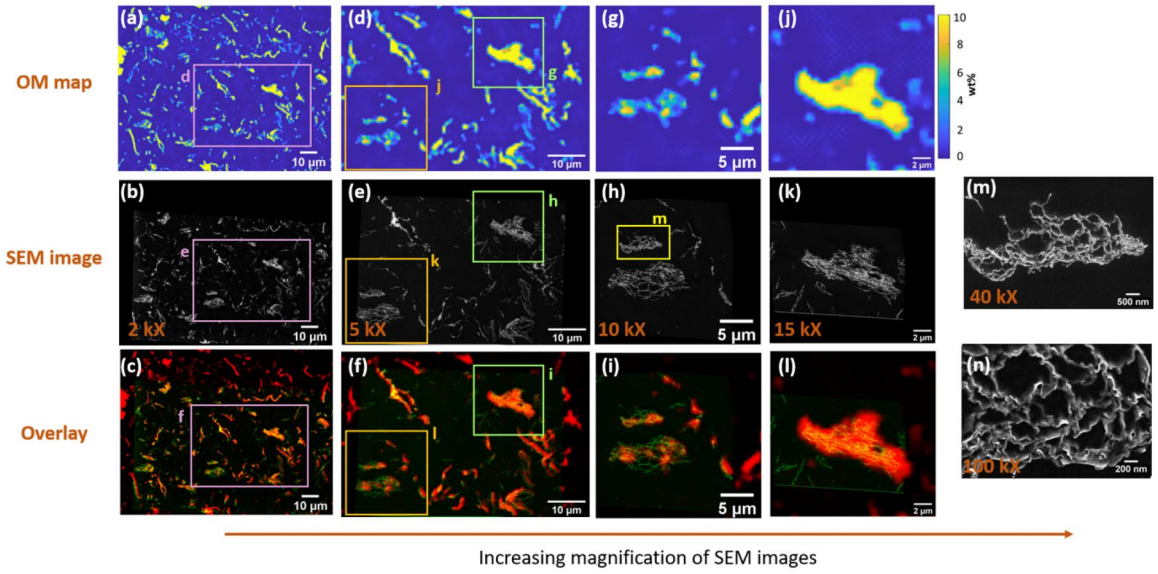


Figure 12. 2D correlative analysis of OM maps and SEM images in 1 wt% GF/epoxy nanocomposites , combined with examples of higher local SEM magnification. (a,d,g,j) Corresponding OM maps of the correlated regions. (b,e,h,k,m,n) SEM images of the targeted regions. (c,f,i,l) Correlated images illustrating the overlay of OM maps and SEM images (red channel: OM map, green channel: SEM images). Color boxes in (a–f,k) depict regions selected for imaging at increasing magnifications.

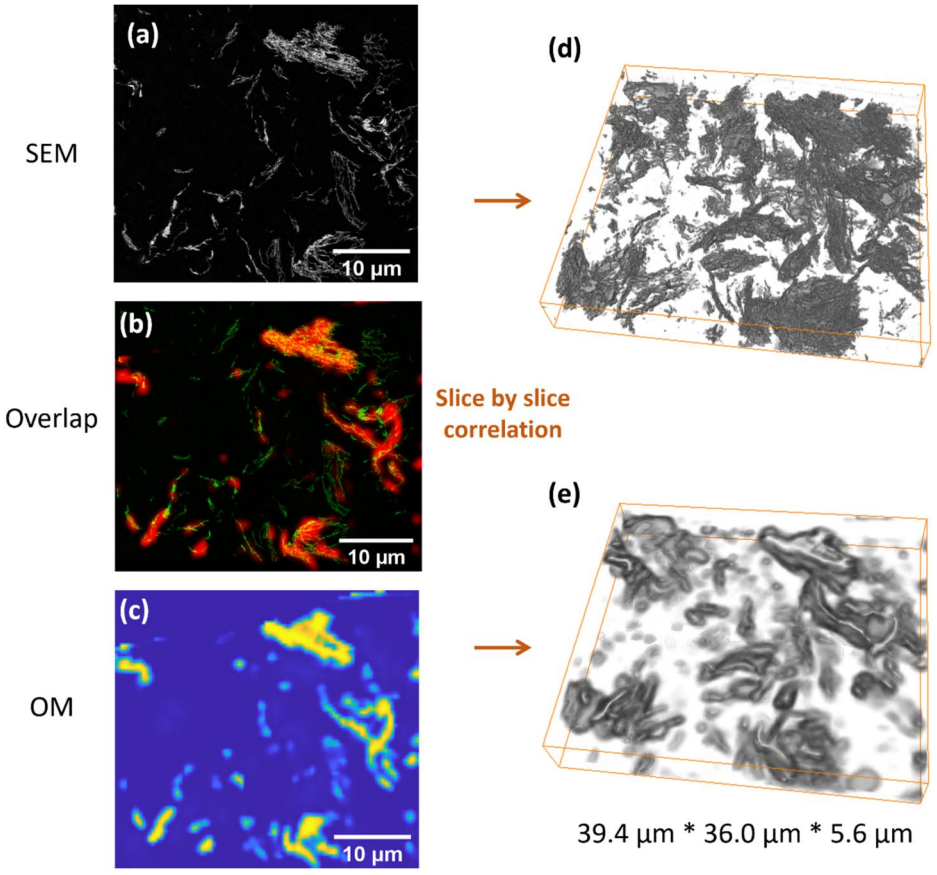


Figure 13. 3D correlative analysis of OM maps and SEM images in 1 wt% GF/epoxy nanocomposites. (a) SEM image of the targeted region. (b) Overlay of the SEM image and OM map. (c) OM map of the selected region. (d) 3D reconstruction of the selected region from SEM images. (e) 3D reconstruction from OM maps (rendered in grayscale).

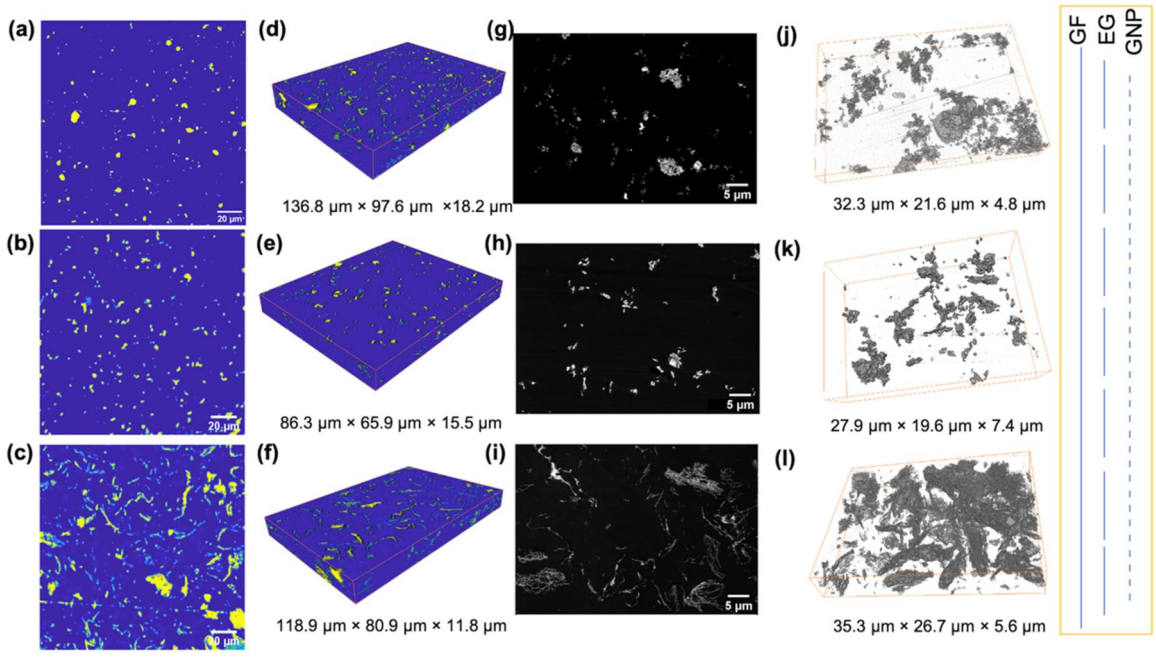


Figure 14. Visualization of representative graphene-related nanocomposites. (a,d,g,j) 1 wt% GNP/epoxy nanocomposites. (b,e,h,k) 1 wt% EG/epoxy nanocomposites. (c,f,i,l) 1 wt% GF/epoxy nanocomposites. (a–c) 2D optical concentration maps. (d–f) 3D optical concentration maps. (g–i) 2D SEM images. (j–l) 3D reconstruction by SEM. The yellow box shows the relative dimensions of the different graphene fillers, in which the height of the dashed lines represents the lateral size of flakes.

local filler volume fraction was extracted (S5, ESI). In comparison, a significant volume of small flakes/thin layers were missing in the optical reconstruction (see slice by slice comparison Video S3). Despite the flake size being large enough to be resolved by OM, in theory, the results demonstrate the complementary value of correlative 3D characterization in providing a complete representation of graphite morphology in composites. While OM itself offers useful insights into the 3D internal structure and general flake location, potentially across very large volumes, integrating it with high resolution SEM enhances accuracy and depth in capturing structural details.

3.6.4. Multiscale structure of graphene-related nanocomposites

The implementation of serial sectioning-based 3D correlative characterization provides complementary information on the multiscale structures of graphene-related nanocomposites. A comprehensive visual representation of the various graphene-related nanocomposites is provided as a summary and guide for future studies (Figure 14). The comparisons show the limitations of commonly applied 2D (optical or electron) microscopic images in structural analysis and the necessity of using 3D techniques to fully understand the characteristics of nanocomposites. The internal 3D structure of graphene-related nanocomposites varies remarkably with different lateral sizes of graphene fillers, which should be carefully considered for each application. The serial-sectioning SEM approach is most suitable for relatively stiff polymer nanocomposites that can be cleanly sectioned by ultramicrotomy. Highly elastomeric matrices may deform during cutting and require additional preparation strategies (e.g. cryo-sectioning). In addition, the accessible volume is limited by the SEM field of view and the number of collected sections, typically corresponding to tens-hundreds of micrometers laterally with depth determined by the number of slices. The entire workflow requires relatively simple instrumentation, including an ultramicrotome and standard microscopes, widely accessible in materials laboratories. The extension of this methodology to general nanomaterials and nanocomposites is also feasible through sample embedding, correlative labeling, and other existing microscopic techniques relevant to a broader range of materials.

4. Conclusions

Understanding the multiscale internal structure of nanocomposites is essential to establish the structure-property relations that underpin materials development for application. This study develops a method for the 3D characterization of graphene-related nanocomposites, based on correlative OM and SEM imaging of serial sections. Samples are preserved as a series of slices, available for repetitive/multi-modal imaging using either technique, facilitating the extraction of rich structural information, or even subsequent local property determinations. To maximize the resolution of the 3D reconstruction using SEM, imaging conditions must be optimized to account for the interplay between acceleration voltage, electron penetration depth, slice thickness, and image contrast. Using the minimum achievable microtomed slice thickness maximizes *z*-resolution; matching the penetration depth (accelerating voltage) to the slice thickness minimizes both charging artifacts and beam damage, whilst imaging all nanoparticles within the slice. Multiscale 3D structures have been successfully reconstructed for representative graphene-related nanocomposites (characteristic filler lateral sizes ranging from sub-micrometre to tens of micrometer). 3D reconstruction using OM provides information of filler distribution, with quantitative measurement of filler concentration. 3D reconstruction using SEM established detailed structural information, including local network connectivity, flake orientation, curvature, and other critical features. Correlative OM and SEM confirms that consistency of the information obtained, but highlights the complementarity of the techniques. In principle, in future, generative AI methods could be used to interpolate realistic high resolution microstructures across the large volume OM data, using the detailed SEM data [51]. The serial sectioning-based correlative methodology will be a powerful tool for investigating materials with multiscale characteristics, such as state-of-the-art hybrids systems (nanocarbon catalyst supports, energy-storage electrodes). The 3D structures are valuable inputs to machine learning or modeling studies, which can in turn assist in the advancement of carbon nanocomposites. The correlative datasets generated in this study are available to stimulate further exploration [52].

Acknowledgments

The authors would like to acknowledge the Harvey Flowers EM suite at Imperial College London for the use of electron microscopes and an ultramicrotome. Yuhan Li is grateful to the China Scholarship Council (CSC) and Imperial College London for funding support.

Author contributions

CRediT: **Yuhan Li**: Conceptualization, Data curation, Formal analysis, Investigation, Validation, Visualization, Writing – original draft; **Milo S. P. Shaffer**: Conceptualization, Formal analysis, Investigation, Methodology, Supervision, Validation, Writing – review & editing.

Disclosure statement

No potential conflict of interest was reported by the author(s).

Funding

Yuhan Li is grateful to the China Scholarship Council (CSC) and Imperial College London for funding support.

Notes on contributors

Yuhan Li received her PhD in Materials from Imperial College London in March 2024. Her doctoral research focused on developing multiscale and multidimensional characterization methodologies for graphene-based structures, integrating advanced microscopy, image processing, and quantitative analysis techniques. In 2025, she began a post-doctoral fellowship at Zhejiang University, where she continues her work on composite materials, with a particular emphasis on functional integration and structural sensing of composite structures.

Milo S. P. Shaffer is a Professor of Materials Chemistry at Imperial College London and was co-Director of the London Center for Nanotechnology (2010–2020). He has extensive experience in carbon and inorganic

nanomaterials synthesis, modification, characterization, and application, particularly for nanocomposite and hierarchical systems, for both structural and electrochemical applications. Notable recent work includes new, patented methods for the dispersion, surface functionalization, and characterization of carbon nanomaterials, and new approaches to the synthesis of functionalized oxide nanoparticles *in situ*.

References

1. Hu K, Kulkarni DD, Choi I, et al. Graphene-polymer nanocomposites for structural and functional applications. Prog Polym Sci. 2014;39:1934. doi: 10.1016/j.progpolymsci.2014.03.001
2. Liew KM, Pan Z, Zhang L-W. The recent progress of functionally graded CNT reinforced composites and structures. Sci China Phys Mech Astron. 2020;63(3):234601. doi: 10.1007/s11433-019-1457-2.
3. Sengupta R, Bhattacharya M, Bandyopadhyay S, et al. A review on the mechanical and electrical properties of graphite and modified graphite reinforced polymer composites. Prog Polym Sci. 2011;36(5):638–670. doi: 10.1016/j.progpolymsci.2010.11.003.
4. Shen X, Zheng Q, Kim J-K. Rational design of two-dimensional nanofillers for polymer nanocomposites toward multifunctional applications. Prog Mater Sci. 2021;115:100708. doi: 10.1016/j.pmatsci.2020.100708.
5. Kumar SK, Krishnamoorti R. Nanocomposites: structure, phase behavior, and properties. Annu Rev Chem Biomol Eng. 2010;1(1):37–58. doi: 10.1146/annurev-chembioeng-073009-100856.
6. Wang Y, Zhang M, Lin A, et al. Mining structure–property relationships in polymer nanocomposites using data driven finite element analysis and multi-task convolutional neural networks. Mol Syst Des Eng. 2020;5(5):962–975. doi: 10.1039/D0ME00020E.
7. Jancar J, Douglas J, Starr FW, et al. Current issues in research on structure–property relationships in polymer nanocomposites. Polymers. 2010;51:3321. doi: 10.1016/j.polymer.2010.04.074
8. Schaefer DW, Justice RS. How nano are nanocomposites? Macromolecules. 2007;40:8501. doi: 10.1021/ma070356w
9. Brown JM, Anderson DP, Justice RS, et al. Hierarchical morphology of carbon single-walled nanotubes during sonication in an aliphatic diamine. Polymers. 2005;46:10854. doi: 10.1016/j.polymer.2005.08.089.
10. Pedrazzoli D, Manas-Zloczower I. Understanding phase separation and morphology in thermoplastic polyurethanes nanocomposites. Polymers. 2016;90:256. doi: 10.1016/j.polymer.2016.03.022.
11. Natarajan B, Lachman N, Lam T, et al. The evolution of carbon nanotube network structure in unidirectional nanocomposites resolved by quantitative electron tomography. ACS Nano. 2015;9(6):6050–6058. doi: 10.1021/acsnano.5b01044.
12. Kashiwagi T, Fagan J, Douglas JF, et al. Relationship between dispersion metric and properties of PMMA/SWNT nanocomposites. Polymers. 2007;48:4855. doi: 10.1016/j.polymer.2007.06.015.
13. Bakshi SR, Batista RG, Agarwal A. Quantification of carbon nanotube distribution and property correlation in nanocomposites. Compos A Appl Sci Manuf. 2009;40(8):1311–1318. doi: 10.1016/j.compositesa.2009.06.004.
14. Zaccardi F, Santonicola MG, Laurenzi S. Quantitative assessment of nanofiller dispersion based on grayscale image analysis: a case study on epoxy/carbon nanocomposites. Compos A Appl Sci Manuf. 2018;115:302–310. doi: 10.1016/j.compositesa.2018.10.003.
15. Glaskova T, Zarrelli M, Aniskevich A, et al. Quantitative optical analysis of filler dispersion degree in MWCNT–epoxy nanocomposite. Compos Sci Technol. 2012;72(4):477–481. doi: 10.1016/j.compscitech.2011.11.029.
16. Zeng Q, Yu A, Lu G. Multiscale modeling and simulation of polymer nanocomposites. Prog Polym Sci. 2008;33(2):191–269. doi: 10.1016/j.progpolymsci.2007.09.002.
17. Kim B, Choi J, Yang S, et al. Multiscale modeling of interphase in crosslinked epoxy nanocomposites. Compos B Eng. 2017;120:128–142. doi: 10.1016/j.compositesb.2017.03.059.
18. Montazeri A, Rafii-Tabar H. Multiscale modeling of graphene- and nanotube-based reinforced polymer nanocomposites. Phys Lett A. 2011;375(45):4034–4040. doi: 10.1016/j.physleta.2011.08.073.
19. Paddock SW. Confocal laser scanning microscopy. Biotechniques. 1999;27(5):992–1004. doi: 10.2144/99275ov01.
20. Smith BE, Yazdani H, Hatami K. Three-dimensional imaging and quantitative analysis of dispersion and mechanical failure in filled nanocomposites. Compos A Appl Sci Manuf. 2015;79:23–29. doi: 10.1016/j.compositesa.2015.08.019.
21. Li S, Li Z, Burnett TL, et al. Nanocomposites of graphene nanoplatelets in natural rubber: microstructure and mechanisms of reinforcement. J Mater Sci. 2017;52(16):9558–9572. doi: 10.1007/s10853-017-1144-0.
22. Lavery LL, Gelb J, Merkle AP, et al. X-ray microscopy for hierarchical multi-scale materials. Microsc Today. 2014;22:16. doi: 10.1017/S155192951400056X.
23. Li Z, Slater TJA, Ma X, et al. The taxonomy of graphite nanoplatelets and the influence of nanocomposite processing. Carbon. 2019;142:99–106. doi: 10.1016/j.carbon.2018.10.043.
24. Garcea SC, Wang Y, Withers PJ. X-ray computed tomography of polymer composites. Compos Sci Technol. 2018;156:305–319. doi: 10.1016/j.compscitech.2017.10.023.
25. Gnanasekaran K, Grimaldi C, With G, et al. A unified view on nanoscale packing, connectivity, and conductivity of CNT networks. Adv Funct Mater. 2019;29(13):1807901. doi: 10.1002/adfm.201807901.

26. Echlin MP, Burnett TL, Polonsky AT, et al. Serial sectioning in the SEM for three dimensional materials science. Curr Opin Solid State Mater Sci. 2020;24:100817. doi: 10.1016/j.cossms.2020.100817.
27. Horstmann H, Körber C, Sätzler K, et al. Serial section scanning electron microscopy (S3EM) on silicon wafers for ultra-structural volume imaging of cells and tissues. PLOS One. 2012;7(4):e35172. doi: 10.1371/journal.pone.0035172.
28. Wacker I, Schroeder RR. Array tomography. J Microsc. 2013;252(2):93–99. doi: 10.1111/jmi.12087.
29. John SF. Multiscale characterisation of particle distribution in nanocomposites across two and three dimensions; 2019.
30. Hashimoto T, Thompson GE, Zhou X, et al. 3D imaging by serial block face scanning electron microscopy for materials science using ultramicrotomy. Ultramicroscopy. 2016;163:6–18. doi: 10.1016/j.ultramic.2016.01.005.
31. Li X, Yang Q, Li H, et al. Quantifying the 3D multiscale dispersion structure of nanofillers in polymer nanocomposites by combining 3D-STEM and synchrotron radiation X-ray CT. Compos B Eng. 2021;212:108687. doi: 10.1016/j.compositesb.2021.108687.
32. Bianco A, Cheng H-M, Enoki T, et al. All in the graphene family – a recommended nomenclature for two-dimensional carbon materials. Carbon. 2013;65:1–6. doi: 10.1016/j.carbon.2013.08.038.
33. Wei J, Vo T, Inam F. Epoxy/graphene nanocomposites – processing and properties: a review. RSC Adv. 2015;5(90):73510–73524. doi: 10.1039/C5RA13897C.
34. Rasband WS. Bethesda (MD); 1997.
35. Schindelin J, Arganda-Carreras I, Frise E, et al. Fiji: an open-source platform for biological-image analysis. Nat Methods. 2012;9(7):676–682. doi: 10.1038/nmeth.2019.
36. Bogovic JA, Hanslovsky P, Wong A, et al. Presented at 2016 IEEE 13th International Symposium on Biomedical Imaging (ISBI); 2016.
37. Drouin D, Couture AR, Joly D, et al. CASINO V2.42: a fast and easy-to-use modeling tool for scanning electron microscopy and microanalysis users. Scanning. 2007;29(3):92–101. doi: 10.1002/sca.20000.
38. Dikin D, Kohlhaas K, Dommett G, et al. Scanning electron microscopy methods for analysis of polymer nanocomposites. Microsc Microanal. 2006;12(S02):674–675. doi: 10.1017/S1431927606067080.
39. Li W, Bauhofer W. Imaging of CNTs in a polymer matrix at low accelerating voltages using a SEM. Carbon. 2011;49(12):3891–3898. doi: 10.1016/j.carbon.2011.05.027.
40. Li W, Buschhorn ST, Schulte K, et al. The imaging mechanism, imaging depth, and parameters influencing the visibility of carbon nanotubes in a polymer matrix using an SEM. Carbon. 2011;49:1955. doi: 10.1016/j.carbon.2010.12.069.
41. Zhao M, Ming B, Kim JW, et al. New insights into subsurface imaging of carbon nanotubes in polymer composites via scanning electron microscopy. Nanotechnology. 2015;26(8):085703. doi: 10.1088/0957-4484/26/8/085703.
42. Burel A, Lavault MT, Chevalier C, et al. A targeted 3D EM and correlative microscopy method using SEM array tomography. Development. 2018;145(12):dev160879. doi: 10.1242/dev.160879.
43. Koike T, Yamada H. Methods for array tomography with correlative light and electron microscopy. Med Mol Morphol. 2019;52(1):8–14. doi: 10.1007/s00795-018-0194-y.
44. Papageorgiou DG, Kinloch IA, Young RJ. Mechanical properties of graphene and graphene-based nanocomposites. Prog Mater Sci. 2017;90:75. doi: 10.1016/j.pmatsci.2017.07.004.
45. Schmidt R, Fitzek H, Nachtnebel M, et al. The combination of electron microscopy, Raman microscopy and energy dispersive X-ray spectroscopy for the investigation of polymeric materials. Macromol Symp. 2019;384(1):1800237. doi: 10.1002/masy.201800237.
46. Carruthers H, Clark D, Clarke FC, et al. Three-dimensional imaging of pharmaceutical tablets using serial sectioning and Raman chemical mapping. J Raman Spectrosc. 2022;53(6):1115–1125. doi: 10.1002/jrs.6337.
47. Böhm T, Moroni R, Thiele S. Serial section Raman tomography with 10 times higher depth resolution than confocal Raman microscopy. J Raman Spectrosc. 2020;51(7):1160–1171. doi: 10.1002/jrs.5878.
48. Fadnavis S. Image interpolation techniques in digital image processing: an overview. Int J Eng Res Appl. 2014;4:70.
49. Fisher SJ, Shaffer MSP. Rapid quantitative mapping of multi-walled carbon nanotube concentration in nanocomposites. Compos Sci Technol. 2018;160:161–168. doi: 10.1016/j.compscitech.2018.03.010.
50. Alekseev A, Chen D, Tkalya EE, et al. Local organization of graphene network inside graphene/polymer composites. Adv Funct Mater. 2012;22(6):1311–1318. doi: 10.1002/adfm.201101796.
51. Dahari A, Kench S, Squires I, et al. Fusion of complementary 2D and 3D mesostructural datasets using generative adversarial networks. Adv Energy Mater. 2023;13(2):2202407. doi: 10.1002/aenm.202202407.
52. Li Y, Shaffer MSP. Dataset: 3D correlative OM and SEM images of graphene nanocomposites. Mendeley Data. 2026;V1. doi: 10.17632/srscfwnrwt.1.